Complex Systems **5** (1991) 1–14

A Multispeed Model for Lattice-Gas Hydrodynamics

Gerald Fahner
Physics Department, Bergische Universität, Gesamthochschule Wuppertal, Gauss-Strasse 20, Postfach 100127, 5600 Wuppertal, Germany

Abstract. A discrete model for two-dimensional hydrodynamics is presented. Compared to previous cellular-automata constructions, it has a richer spectrum of states and is thus closer to molecular dynamics. First, the model is tested regarding equilibrium isotropy. Next, thermal effects in equilibrium are discussed. Then the lattice gas is used to model the two-dimensional incompressible Navier-Stokes equation by performing a Poiseuille flow experiment. The expected effect of the system size on viscosity is found. For the shear flow we observe a breakdown of isotropy—much stronger than that of the equilibrium distribution—appearing as a direction-dependent viscosity. The viscosity is computed from the nonequilibrium distributions, and agreement with the simulation results is found.

1. Description of the model

Our lattice gas is discrete in space, time, and state, and lives on a quadratic lattice. It is known that with this geometry there arise some problems concerning spurious invariants and isotropy [1, 2], if velocities are restricted to $\vec{v} = (\pm 1, 0)$ and $\vec{v} = (0, \pm 1)$. The spurious invariants can be eliminated by adding more velocities, including rest particles with $\vec{v} = 0$. It is the purpose of the present paper to study the extent to which the anisotropy effects can be suppressed by including the larger velocity spectrum shown in figure 1. On each site there are 21 allowed single-particle states that may be either empty or occupied by at most one particle with unit mass, so 2^{21} microconfigurations are possible on a single site. This exclusion principle allows cheap storage and easy handling of data. The time development proceeds as usual with a translation step followed by a collision step, each step applied synchronously to all particles. Collisions take place between particles on the same site. Particles crossing or overtaking during a translation step do not undergo a collision.

The collision rules are designed to conserve particle number, momentum, and energy. The quadruple (N, E, P_x, P_y) defines for each site a local "macrostate." The collision step proceeds as follows: For each site, the

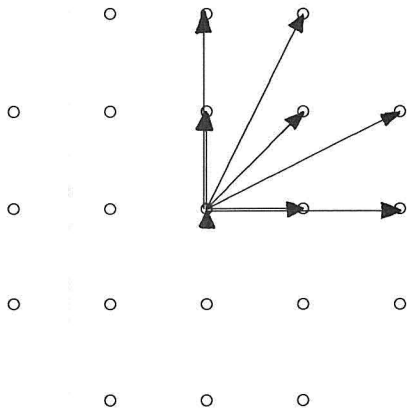

Figure 1: Spectrum of velocities. Only velocities in the first quadrant are indicated by arrows.

macrostate of the incoming particle configuration is computed. Then an output configuration is chosen randomly among all microconfigurations compatible with this macrostate. These configurations are either stored directly as bit patterns in a look-up table or constructed from one of the stored bit patterns by using lattice symmetries or particle-hole symmetry.

To retain microreversibility, it is necessary to have all microconfigurations that are compatible with an (N, E, P_x, P_y) accessible to the outgoing particles, *if* this macrostate is allowed to undergo a collision. Because of the combinatorial explosion of microstates with increasing N, we thus restrict collisions to situations with $N \leq 5$ particles. Accordingly we work with particle densities $\langle N \rangle \sim 2$. Then collisions may take place in almost all cases and efficient updating, short mean free paths, and quick relaxation into local equilibrium should be guaranteed. Another way to avoid combinatorial explosion would be to collide the particles on a site pair-wise and to work off all pairs, but this would make the collision process computationally more difficult.

2. The equilibrium distribution

We start with the maximum entropy principle for the occupation numbers n_i on a single site, where $i = 1, \ldots, 21$. Here i denotes one of the allowed tuples (v_{ix}, v_{iy}). Under constraints of fixed average values for

$$\text{number of particles per site} \quad N = \sum_{i=1}^{21} n_i \tag{2.1}$$

$$\text{momentum per site} \quad \vec{P} = \sum_{i=1}^{21} \vec{v}_i n_i \tag{2.2}$$

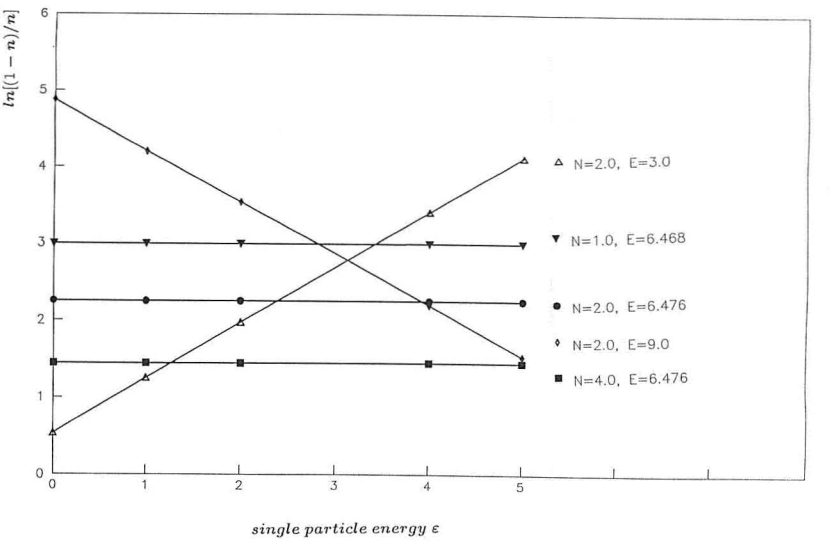

Figure 2: Test of the Fermi distribution for different system parameters. The solid lines are the theoretical predictions from equation (2.4).

$$\text{energy per site} \quad E \;=\; \sum_{i=1}^{21} \varepsilon_i n_i \tag{2.3}$$

with single-particle energies $\varepsilon_i \equiv v_{ix}^2 + v_{iy}^2 \in \{0, 1, 2, 4, 5\}$, we obtain a Fermi function for the occupation numbers:

$$n_i = \frac{1}{1 + z \exp\left(\beta\varepsilon_i - \vec{\alpha}\vec{v}_i\right)} \tag{2.4}$$

where $z = \exp\left(-\beta\mu\right)$ and where the Lagrangian multipliers μ, $\vec{\alpha}$, and β are functions of the conserved quantities. Notice that here and in the following, E, N, and $\vec{P}$ are average quantities per lattice site.

The occupation numbers for different values of E and N and for vanishing mean momentum $\vec{P}$ were measured and are plotted in figure 2. For each choice of N and E we thermalized a 32×16 system at rest and then averaged over 10^4 iterations.

Notice that negative temperatures are allowed since there is an upper bound for the particle energies. For very low and very high energies per particle, the Fermi gas is degenerated. But in order to obtain good isotropy properties, the whole spectrum of directions should be excited. In the following we will assume nearly equal excitation of all states, characterized by $T \equiv 1/\beta \simeq \infty$ and $E \approx E_0 \equiv (N/21)\sum_i \varepsilon_i$. By symmetry, $\vec{\alpha}$ must vanish for $\vec{P} = 0$. To describe low-speed equilibria we restrict ourselves to small values of α. With this parameter adjustment, then by inserting equation (2.4) into the conservation equations and by neglecting terms

$O((E-E_0)^2, P^2(E-E_0), P^4)$, we get

$$z = -1 + \frac{1}{N}\left\{21 + \frac{17\,(21)^2 f}{N}\right\} \tag{2.5}$$

$$\beta = -\frac{(21)^3}{4N(21-N)}\left\{f - \frac{g}{34}P^2\right\} \tag{2.6}$$

$$\alpha_{x(y)} = \frac{(21)^2}{34N(21-N)}\left\{1 - \frac{71(21)^2 g}{2}\left[f - \frac{g}{34}P^2\right]\right\}$$
$$P_{x(y)} - \frac{(21)^3}{(34)^4 N^3}[rP^2_{x(y)} + sP^2_{y(x)}]P_{x(y)} \tag{2.7}$$

with

$$f \equiv \frac{(E-E_0)}{335} \qquad g \equiv \frac{21-2N}{34N(21-N)}$$
$$r \equiv -\frac{107}{6} + 36\frac{N(21-N)}{(21)^2} \qquad s \equiv -\frac{105}{6} + 34\frac{N(21-N)}{(21)^2}$$

In contrast to the results for the hexagonal lattice [3, 4], there is a difference between the coefficients r and s that appear in equation (2.7), reflecting the anisotropy of the square lattice. But this difference is very small. For equal excitation we thus could hope that anisotropy is indeed negligible at low speeds, since moreover its effect ceases for vanishing P. To check the analytic results we performed some simulations with different uniform stream velocities in directions parallel and diagonal to the square lattice. The data shown in figures 3 and 4 are for parallel and diagonal flows with $N = 2$ and $E = 6.476 \simeq E_0$. For each P we used 10^4 iterations on a 128×64 lattice. In addition to the mean populations of different single-particle states, the figures show solid curves predicted by equations (2.4) through (2.7).

The experimental data points lie well on the curves predicted by theory. In the following simulations the magnitude of P will be so small (< 0.06) that the above equilibrium anisotropy should not show up.

3. A Poiseuille flow experiment

To test the hydrodynamic behavior of the model, we simulated a channel flow designed similarly to that described in [5]. A stationary flow is driven by an average rate $\langle \Delta P \rangle$ of momentum added uniformly to a channel between two walls. This is done by flipping velocities at randomly chosen sites and times. Figure 5 shows all flips used to add momentum for the axis-parallel flow. ΔP denotes the units of momentum added to the system when a flip takes place. In addition to the flips shown, all flips obtained by inflections on the x-axis are used. If at the chosen space-time point one or several flips can be applied, one of them is chosen randomly; otherwise we go to the next neighbor downstream. Thus, at each site a uniform force $G = \langle \Delta P \rangle / (\text{system size})$ is simulated. The walls and the force are parallel to the

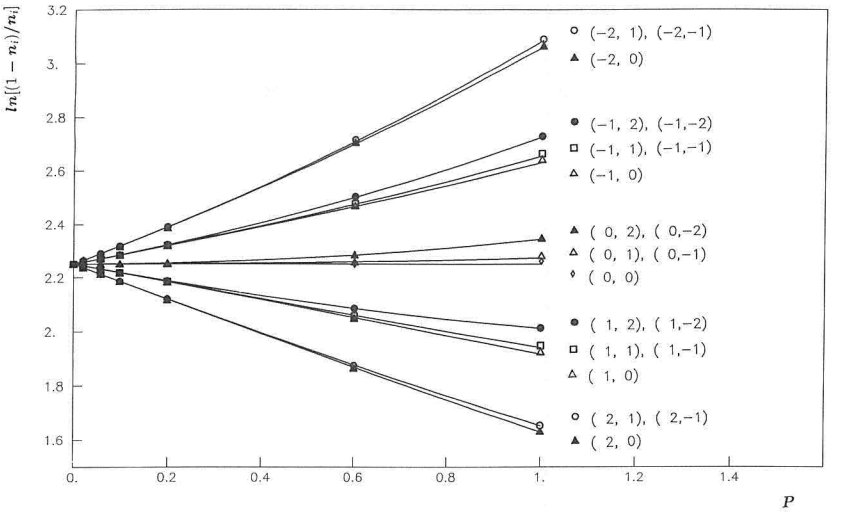

Figure 3: Transformation of the Fermi distribution for uniform flows parallel to one axis of the square lattice.

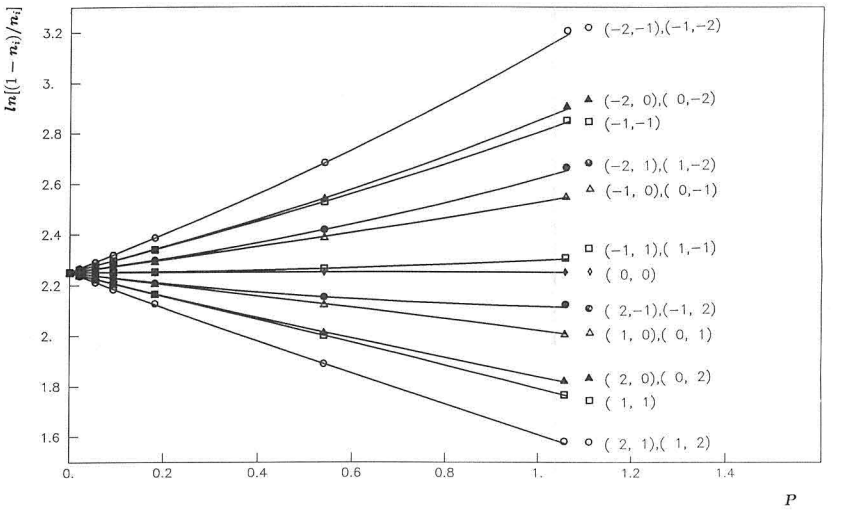

Figure 4: The same as figure 3, but for a diagonal flow on the square lattice.

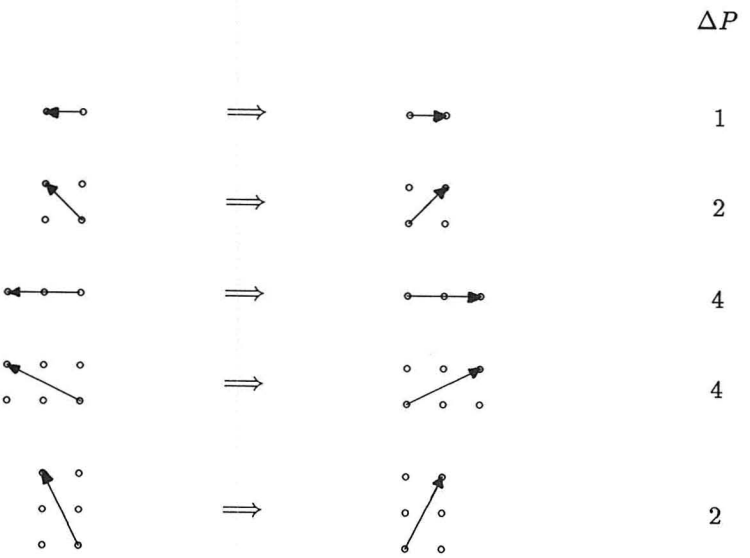

Figure 5: Velocity flips used with equal probability to add momentum for the Poiseuille flow parallel to an axis.

x-direction. At the walls momentum is dissipated via Moebius boundary conditions [5]. Their effect is to reverse the tangential components, but not the normal components, of the velocities of all particles crossing or arriving at the wall layer. Figure 7 shows the action of the wall layer on velocities of particles that *cross* the wall. The solid arrows are snapshots before and the dashed ones after crossing. In addition to the crossings shown, all crossings obtained by inflection on the normal component of the wall and on the wall itself are used. Not shown are particles arriving at a wall site; after inflection of their tangential component they simply continue their voyage from the same site. Particles penetrating through the wall in the described way then reappear at the opposite lattice side via periodic boundary conditions. The periodicity allows us to simulate the channel flow using only *one* wall layer. The channel ends are simply wrapped periodically. After averaging over many iterations we obtain a stream profile $P_x(y)$ of the momentum density (see figure 9).

In different experiments we varied the mean flow velocity and the lattice size. All the results agree well with the parabolic continuum solution

$$P_x(y) = C_1 + C_2 y + C_3\, y^2 \tag{3.1}$$

$$C_3 = -G/2\nu \tag{3.2}$$

y : distance from the wall

ν : kinematic viscosity

ν is obtained from the curvature of the parabola fitted through $P_x(y)$. The

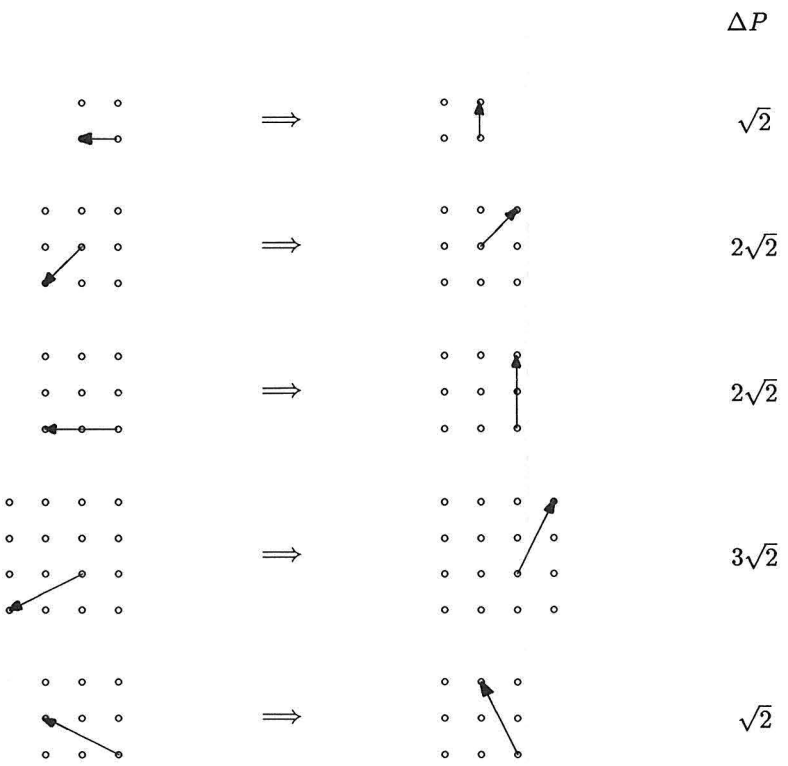

Figure 6: The same as figure 5, but for diagonal flow.

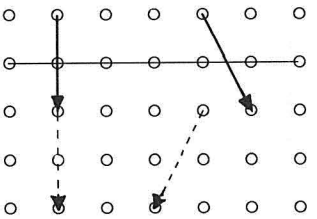

Figure 7: Friction at the wall for parallel flow.

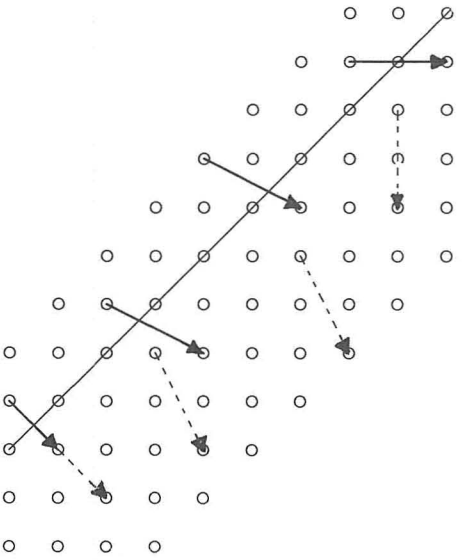

Figure 8: The same as figure 7, but for diagonal flow.

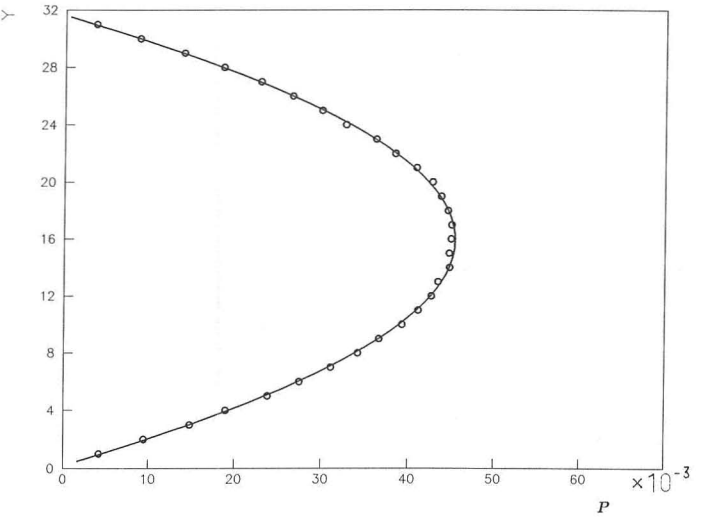

Figure 9: Typical stream profile for a 64×32 lattice and for $\langle \Delta P \rangle = 1$, obtained from averaging over 8×10^5 iterations. The solid line is the best fit by a parabola.

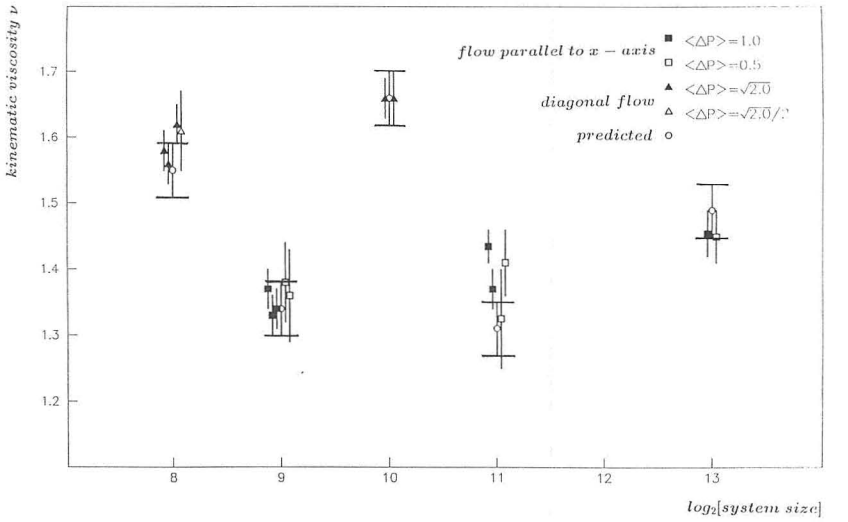

Figure 10: Viscosities obtained by simulations and predicted using the nonequilibrium distribution.

wall layer at $y = 0$ was not used for the fit because the parabolic profile is somewhat disturbed there. Figure 10 shows the results for ν obtained from equation (3.2) for different simulation runs with lattice sizes $16\sqrt{2} \times 8\sqrt{2}$ through 128×64, different forcing strengths $\langle \Delta P \rangle$, and different flow directions. For a fixed system size we find no dependence of the viscosity on the stream velocity or on the forcing strength, and thus conclude that we measure the response of an unperturbed system. But we see that ν increases with the system size, an effect discussed in detail in [5].

In addition, we performed an isotropy test by repeating the experiment with walls and forces diagonal to the square lattice. The allowed velocity flips and the effect of the walls for this case are shown in figures 6 and 8. Again parabolic profiles are obtained, but the viscosities ν_D for the diagonal flow are somewhat different from the ν_P measured for the parallel flow. The ν_D were indeed obtained from lattices with domains differing from those for the ν_P. For ν_D we used the sizes $16\sqrt{2} \times 8\sqrt{2}$ and $32\sqrt{2} \times 16\sqrt{2}$, whereas for ν_P we used 32×16, 64×32, and 128×64. But as can be seen from figure 10, the increase in viscosity with the lattice domain is a small effect compared to its direction dependence. This phenomenon indicates a breakdown of isotropy in the stressed medium and will be discussed in more detail in the next section.

4. Viscosity and nonequilibrium distributions

In this section we study the effect of perturbing the velocity distribution using a shear flow, and a computation of the viscosity from it. More precisely, we choose $P_y = 0$ and assume that P_x grows linearly with y. For the following,

let $\beta = 0$. If we assume the gradient $P_{x,y} = \partial P_x/\partial y$ is small, the local equilibrium description will still be approximately valid. For a shear flow $\vec{P}(\vec{x}) = (k \cdot y, 0)$ with $k \ll 1$, we may then write

$$n_i(\vec{x}) = n_i^0 + n_i^u(y) + n_i^s(y) \tag{4.1}$$

with

$$n_i^0 = \frac{N}{21} \equiv d \tag{4.2}$$

$$n_i^u(y) = \frac{\partial n_i}{\partial P_x} P_x(y) \equiv c \cdot v_{ix} \cdot y \cdot P_{x,y} \tag{4.3}$$

Here $n_i^s(y)$ is the perturbation due to the shear. The first two terms in equation (4.1) come from equation (2.4) developed to first order in P_x. From equations (2.4) and (2.7) we have $c = (1/v_{ix})(\partial n_i/\partial \alpha_x)(\partial \alpha_x/\partial P_x) = 1/34$ independently of N. The mechanism responsible for the perturbation n_i^s may be motivated as follows: Consider a site positioned for simplicity at $y_0 = 0$. Then we have $n_i^u(y_0) = 0$. The $n_i(y_0)$ are the probabilities for *incoming* velocities v_i at y_0. Due to the increase in n_i^u with y, we expect a particle arriving from above is more likely to have a positive v_x, whereas a particle coming from below is more likely to have a negative v_x. The sign of the correction n_i^s induced thereby must change with v_{ix}, v_{iy}, and $P_{x,y}$. The simplest ansatz is thus

$$n_i^s = -a \cdot v_{ix} \cdot v_{iy} \cdot P_{x,y} \tag{4.4}$$

with a constant $a > 0$. Notice that n_i^s does not contribute to the conserved quantities (2.1) through (2.3). Ansatz (4.4) was verified in the above Poiseuille experiment for a flow parallel to the lattice. In particular, it was checked that the coefficient a does not depend on the absolute value of v_i. For the Poiseuille flow, the gradient is of course not constant; rather, $k \propto y$, so a could be determined from the slope of the straight lines in figure 11. The open symbols shown there represent the quantities $\langle n^s \rangle$ defined in equation (4.5) and are obtained using 4×10^5 iterations. The straight lines are linear fits predicted by equation (4.4). To determine the corrections n_i^s, the states were lumped into three groups with velocities

$$\{(v_x, v_y), (-v_x, v_y), (-v_x, -v_y), (v_x, -v_y)\} \qquad v_x, v_y \neq 0$$

Then for each group

$$\langle n^s \rangle = \frac{1}{4} \mid n_{x,y} + n_{-x,-y} - (n_{x,-y} + n_{-x,y}) \mid \tag{4.5}$$

was computed. In summing over these four states obtained by reflection, the background terms n^0 and n^u cancel by symmetry. Our simulation results for a 64×32 lattice are shown in figure 11 and agree well with (4.4). Notice that, a priori, a could depend on the energies of the states, but does not within our errors.

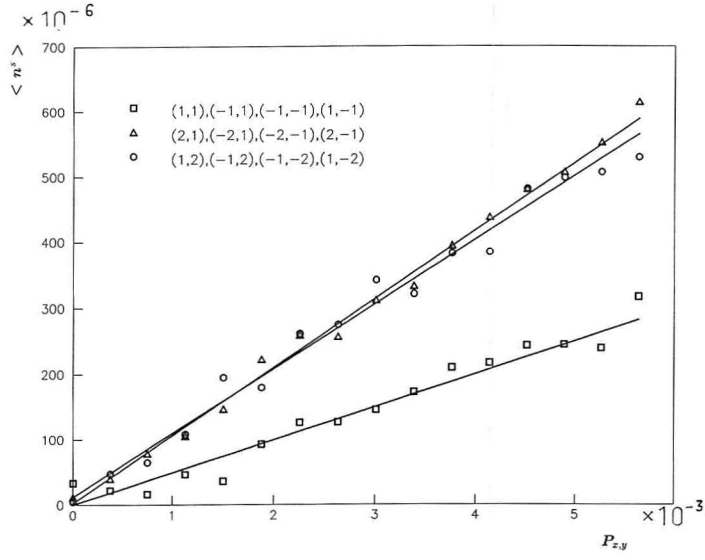

Figure 11: Check of ansatz (4.4) for parallel shear stress.

In order to obtain an expression for the viscosity, consider a site at $y_0 = 0$. Following [6], we denote by Q the momentum flow downwards through a segment of unit length parallel to the x-axis and located between y_0 and $y_0 + 1$ (see figure 12). Obviously,

$$Q = \left\{ \sum_{i:v_{iy}<0} - \sum_{i:v_{iy}>0} \right\} n_i(y_i) v_{ix} \tag{4.6}$$

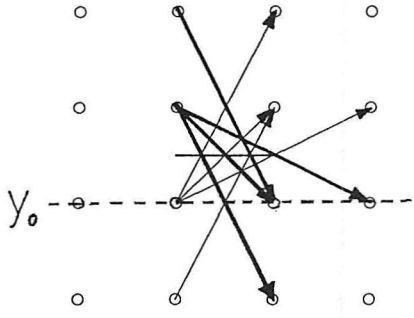

Figure 12: Momentum transport through a unit segment parallel to the x-axis. Only velocities pointing into positive x-direction are indicated.

with the y-coordinates of the sites where the *incoming* particles arrive denoted by y_i. Inserting here our expansion

$$n_i(\vec{x}) = d + c \cdot v_{ix} \cdot y \cdot P_{x,y} - a_P \cdot v_{ix} \cdot v_{iy} \cdot P_{x,y} \tag{4.7}$$

with a coefficient a_P for the *parallel* flow rather than a general a, we get

$$Q = (-18c + 36a_P)P_{x,y} \tag{4.8}$$

By comparison with $Q = \nu P_{x,y}$ from the definition of the viscosity, we find

$$\nu_P = -18c + 36a_P \tag{4.9}$$

For a flow along the diagonal of the lattice, we make an ansatz analogous to (4.7), but now with a different constant a_D:

$$n_i(\vec{x}) = d + c \cdot v_{ix} \cdot y \cdot P_{x,y} - a_D \cdot v_{ix} \cdot v_{iy} \cdot P_{x,y} \tag{4.10}$$

This complication derives from our breaking of rotational invariance. Simulations show indeed that for lattices of comparable size we get different constants a, for example,

$$\begin{aligned} a_P &= 0.051 \pm 0.001 \quad \text{for axis-parallel flow on a } 64 \times 32 \text{ lattice} \\ a_D &= 0.062 \pm 0.001 \quad \text{for diagonal flow on a } 32\sqrt{2} \times 16\sqrt{2} \text{ lattice} \end{aligned}$$

In both cases, a was obtained by means of equation (4.5). For the viscosity of a diagonal flow, an argument analogous to the above gives

$$\nu_D = -\frac{35}{2}c + \frac{70}{2}a_D \tag{4.11}$$

The coefficients a were determined for all system sizes considered so far, using 2×10^5 through 4×10^5 iterations per sample. The viscosities derived from equations (4.9) and (4.11) are also shown in figure 10. They agree very well with those measured directly. Notice that the system-size dependence of the viscosity is indeed correctly captured. From the expressions (4.9) and (4.11) for the viscosities we see that the main source for the discrepancy between ν_P and ν_D is the difference between the coefficients a_P and a_D. This indicates that it is the shear induced difference in the occupation numbers that is responsible for the anisotropy. The isotropy of the equilibrium distribution depends only on the isotropy of the single-particle spectrum (which is very good), whereas the nonequilibrium distribution depends also on the less isotropic collisions. Relaxation to equilibrium is due to collisions, so they play a role in damping shear induced corrections of the incoming particle distribution. The coefficient a is closely related to the degree of this damping [6]. When shear parallel to the lattice axes is present, collisions are more efficient in dissipating these perturbations than when there is diagonal shear stress. This shortens the distance over which propagating momentum is transferred for the parallel Poiseuille flow, and thus yields a lower value for the viscosity.

5. Conclusions

We studied some properties of a multi-velocity lattice gas on a square lattice. By including a rich velocity spectrum our model comes closer to traditional molecular dynamics than previous models. It also allows simulation of thermal effects. A three-dimensional version of our model would use the simple cubic lattice and aim at improving its insufficient symmetries by using many velocities of different moduli. This seems a natural extension compared to the pseudo-three-dimensional analog [9] of the FHP model [3]. The latter extension achieves built-in isotropy by choice of a suitable but somewhat artificial geometry. However, the degree of isotropy that can be achieved by averaging over many velocities has to be studied carefully.

We stated the problem in two dimensions and were mostly interested in the effect of the many velocities in partly restoring broken Galilei invariance and rotational symmetry of the quadratic lattice. For equal excitation of all energy states we obtained good equilibrium isotropy. In spite of this, we observed that isotropy is broken to a much larger degree when shear stress is present. The phenomenon that nonequilibrium states might be more sensitive to the breaking of a basic symmetry than equilibrium states was also found by [7]. It seems to be a general danger of lattice gas models that should be given more attention [8, 10]. Notice that there seems to be a simple possibility to improve nonequilibrium isotropy in our model: For $N = 2$ and $E/N = 4$, where high energy states are preferred, we measure viscosities $\nu_P = 1.57 \pm 0.06$ for a 32×16 lattice and $\nu_D = 1.62 \pm 0.06$ for a $16\sqrt{2} \times 8\sqrt{2}$ lattice. The unexpectedly large anisotropy effects indicate that care must be taken when using this or simpler models on the square lattice for modeling thermal effects.

Acknowledgments

I am very much indebted to P. Grassberger for stimulating this work, giving useful hints and helping me with the manuscript.

References

[1] J. Hardy, Y. Pomeau, and O. de Pazzis, "Time Evolution of a Two-Dimensional Model System. I. Invariant States and Time Correlation Functions," *Journal of Mathematical Physics*, **14** (1973) 1746.

[2] J. Hardy, O. de Pazzis, and Y. Pomeau, "Molecular Dynamics of a Classical Lattice Gas: Transport Properties and Time Correlation Functions," *Physical Review A*, **13** (1976) 1949.

[3] U. Frisch, B. Hasslacher, and Y. Pomeau, "Lattice Gas Automata for the Navier-Stokes Equation," *Physical Review Letters*, **56** (1986) 1505.

[4] S. Wolfram, "Cellular Automaton Fluids 1: Basic Theory," *Journal of Statistical Physics*, **45** (1986) 471.

[5] L. P. Kadanoff, G. R. McNamara, and G. Zanetti, "A Poiseuille Viscosimeter for Lattice Gas Automata," *Complex Systems*, **1** (1987) 791.

[6] M. Hénon, "Viscosity of a Lattice Gas," *Complex Systems*, **1** (1987) 762.

[7] J. Dahlburg, D. Montgomery, and G. Doolen, "Noise and Compressibility in Lattice Gas Fluids," *Physical Review A*, **36** (1987) 2471.

[8] B. Chopard and M. Drosz, "Cellular Automata Model for Thermo-Hydrodynamics," in *Chaos and Complexity*, edited by R. Livi (World Scientific, Singapore, 1988).

[9] D. d'Humières, P. Lallemand, and U. Frisch, "Lattice Gas Models for 3D Hydrodynamics," *Europhysics Letters*, **2** (1986) 291.

[10] D. A. Wolf-Gladrow, R. Nasilowski, and A. Vogeler, "Numerical Simulations of Hydrodynamics with a Pair Interaction Automaton in Two Dimensions," *Complex Systems*, **4** (1990) 139.